



# Design, fabrication, and cold test of an S-band high-gradient accelerating structure for compact proton therapy facility

Yu Zhang<sup>1,2,3</sup> · Wen-Cheng Fang<sup>1,4</sup> · Xiao-Xia Huang<sup>1,4</sup> · Jian-Hao Tan<sup>1,4</sup> ·  
Cheng Wang<sup>1,2</sup> · Chao-Peng Wang<sup>2</sup> · Zhen-Tang Zhao<sup>1,2,3,4</sup>

Received: 23 November 2020 / Revised: 17 January 2021 / Accepted: 18 January 2021 / Published online: 16 April 2021  
© China Science Publishing & Media Ltd. (Science Press), Shanghai Institute of Applied Physics, the Chinese Academy of Sciences, Chinese Nuclear Society 2021

**Abstract** An S-band high-gradient accelerating structure is designed for a proton therapy linear accelerator (linac) to accommodate the new development of compact, single-room facilities and ultra-high dose rate (FLASH) radiotherapy. To optimize the design, an efficient optimization scheme is applied to improve the simulation efficiency. An S-band accelerating structure with 2856 MHz is designed with a low beta of 0.38, which is a difficult structure to achieve for a linac accelerating proton particles from 70 to 250 MeV, as a high gradient up to 50 MV/m is required. A special design involving a dual-feed coupler eliminates the dipole field effect. This paper presents all the details pertaining to the design, fabrication, and cold test results of the S-band high-gradient accelerating structure.

**Keywords** S-band · High gradient · Accelerating structure · Compact · Single-room facility · Dual-feed coupler · Cold test

## 1 Introduction

Proton therapy, which constitutes approximately 85% of hadron therapy, is currently the main hadron therapy for the daily treatment of tumors. The history of proton therapy can be traced back to 1946, when Robert Wilson proposed the use of proton beams produced by an accelerator to treat human tumors [1, 2]. The two main delivery techniques currently used for proton therapy are passive scattering and pencil beam scanning systems (also known as active scanning systems) [2]. As of July 2020, approximately 104 facilities are dedicated to proton or heavy ion therapy worldwide [3]. More than 3 million new cancer patients are diagnosed in China every year [4]. Therefore, it is crucial to develop proton therapy in China.

Three types of classic accelerators can be used to accelerate protons: cyclotrons, synchrotrons, and linear accelerators (linacs). Although cyclotrons and synchrotrons are typically used for proton therapy as mutual products because they can be used in compact, single-room facilities, and they satisfy new ultra-high dose rate (FLASH) radiotherapy requirements, proton therapy solutions based on linacs can achieve better performances. This is because, for compact systems, the facility can be folded into two upper and lower layers, thereby significantly reducing the overall size of the device and satisfying the requirement for a single-room facility, as shown in Fig. 1. FLASH-RT involves delivering large doses of radiation (20–30 Gy) for a single treatment in less than 100 ms, at mean dose rates above 100 Gy/s [5], which may be achieved only using a linac. In addition, linacs offer other advantages, including short time required for energy modulation, small output beam size and emittance, relatively simple control system, and effective acceleration and control of the beam.

This work was supported by the Alliance of International Science Organizations (No. ANSO-CR-KP-2020-16).

✉ Wen-Cheng Fang  
fangwencheng@zjlab.org.cn

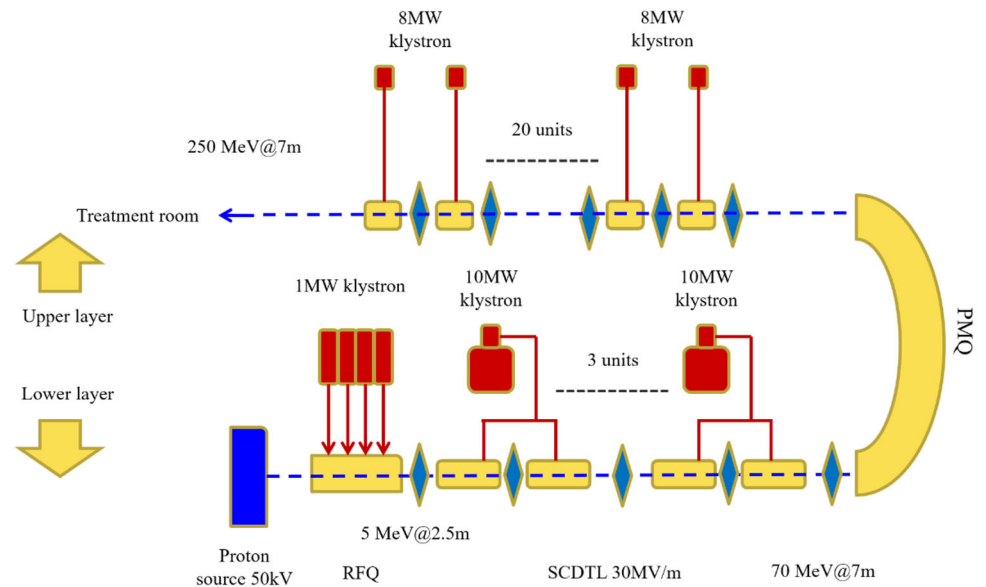
<sup>1</sup> Shanghai Institute of Applied Physics, Chinese Academy of Sciences, Shanghai 201800, China

<sup>2</sup> University of Chinese Academy of Sciences, Beijing 100049, China

<sup>3</sup> ShanghaiTech University, Shanghai 201210, China

<sup>4</sup> Shanghai Advanced Research Institute, Chinese Academy of Sciences, Shanghai 201204, China

**Fig. 1** (Color online) Layout of all-linac scheme



In the 1990s, a linac solution for proton therapy named PL-66 was first proposed by the Fermi National Laboratory in the United States [6, 7]. The optimized solution following PL-250 was the first full-energy design for proton therapy linacs, but no prototype has yet been developed [6]. Subsequently, several facility proposals, such as LIBO (Linac Booster), LIGHT (Linac for Image Guided Hardon Therapy), and TOP-IMPLART (Intensity Modulated Proton Linear Accelerator for Radio-Therapy) were developed [8, 9]. Recently, the TULIP project for a single-room facility was designed in collaboration with the CLIC team of CERN. TULIP is the latest compact high-gradient proton therapy linac device with a single room, measuring only  $22\text{ m} \times 9\text{ m}$ . The high-gradient accelerating structure adopts a backward traveling wave (BTW) structure with an average gradient of  $50\text{ MV/m}$ , and the energy range of the accelerator is  $70\text{--}230\text{ MeV}$  [10].

In this study, we investigated a high-gradient accelerating structure that can achieve a smaller size, more compactness, and higher flow intensity. Additionally, it can be used in single-room facilities and FLASH therapy. An S-band linac structure with an accelerating gradient greater than  $50\text{ MV/m}$  is currently being developed to accommodate future compact proton therapy facilities. In this study, we aim to demonstrate this accelerating gradient in cold tests and, if the experimental conditions permit, we hope to conduct a high-power test in the future. For simplicity, the accelerating structure designed in this program was a single-period structure operating at  $2856\text{ MHz}$  with an operating model of  $\pi$ . In the future, we may further investigate the biperiodic standing wave (SW) accelerating structure owing to its high stability [11]. This paper introduces an S-band SW accelerating structure, including its accelerating cavity design and specific coupler design. Because the

S-band SW accelerating structure has a higher shunt impedance than the BTW accelerating structure, a higher energy gain can be obtained. The design of the structure is based on an efficient method known as structure optimization by polynomial fitting (SOPF), which can simplify complicated electromagnetic simulations via a rapid numerical procedure [12]. Furthermore, the design of a dual-feed coupler that can eliminate dipole fields, reduce the power flow of the coupler and waveguide, and effectively reduce the maximum electromagnetic field is presented herein. Finally, the process and results of the cold tests are provided.

## 2 Requirements of compact linac

The investigated S-band SW accelerator for a high-gradient linac proton therapy facility comprises a proton source, an RFQ, an SCDTL, an accelerating structure, a klystron, and a permanent magnet quadrupole (PMQ). The injector of the facility includes a proton source, an RFQ, and an SCDTL to achieve a fixed energy of  $70\text{ MeV}$ . The main accelerator uses the SW acceleration mode to accelerate the proton energy from  $70$  to  $250\text{ MeV}$ . By modulating the power source of the klystron, the linac energy range of  $70\text{--}250\text{ MeV}$  can be adjusted. For focusing, the linear accelerator adopts a PMQ design. The S-band accelerating structure with a frequency of  $2856\text{ MHz}$  was designed with a low beta of  $0.38$ , which is a difficult structure to achieve for proton therapy linacs. The layout of the all-linac scheme is illustrated in Fig. 1. The main accelerator comprised 20 accelerating units and several permanent magnets. Its length was approximately  $7\text{ m}$ .

**Table 1** Main geometric and SW accelerating parameters for  $\beta = 0.38$ 

Particle	Protons
Input energy (MeV)	70
Output energy (MeV)	80
Pulse length ( $\mu\text{s}$ )	5
Operating mode	$\pi$
Operating frequency (GHz)	2.856
Number of accelerating cells	11
Beam aperture (mm)	1
Structure active length $L$ (mm)	< 250
Design accelerating gradient $E_a = E_0 T T$ factor (MV/m)	50
Maximum ratio surface $E$ -field to accelerating gradient $E_s/E_a$	4
Maximum ratio surface $H$ -field to accelerating gradient $H_s/E_a$ (mA/V)	4
Maximum ratio $S_c$ to accelerating gradient square $S_c/E_a^2$ (A/V)	$2.7 \times 10^{-4}$
Breakdown rate (per pulse)	$10^{-6}$
Temperature rise $\Delta T$ (K)	< 40
Klystron power (MW)	8

All previous developments of linacs for proton therapy have focused on the efficient acceleration and control of the beam. In recent years, dimensions have become increasingly important, since the ultimate goal is to have proton therapy facilities in hospitals, and the requirement of single-room facility is increasing [3]. To create a shorter accelerator, TERA Foundation in collaboration with the CLIC group at CERN has launched a high-gradient research campaign to investigate the high-gradient limit of S-band accelerating structures [13–15]. Based on the tests results, a high-gradient BTW accelerating structure for  $\beta = 0.38$  was built and tested. This development allowed the length of the linac that must be mounted on the rotating structure to be halved, thereby reducing size, weight, and ultimately costs [16, 17].

To fulfill the requirements of the entire equipment, such as sufficient compactness, miniaturization, reliability, easy operation, sufficient energy and dose for short-term treatment, safety, and easy maintenance, the appropriate accelerating structure must be selection and then optimized. For the accelerating section, we adopted the S-band SW accelerating structure, which was designed with a low beta of 0.38. A design scheme was proposed, and the desired specifications for the designed S-band high-gradient accelerating structure, as listed in Table 1, was satisfied. The specifications were based on those of the high-gradient linear accelerating structure designed by TULIP for proton therapy [10].

### 3 RF design and optimization

The design and optimization of an accelerating structure are complicated and extensive. The traditional optimization method adopts a strict step-by-step approach to optimize multiple parameters. If the final design fails to satisfy certain performance targets, then all the optimization calculations must be re-performed, thereby resulting in an extremely slow and laborious design process. To render the optimization process simpler and more accurate, we adopted an efficient optimization method for polynomial fitting, in which multiple objects are optimized automatically for high gradient and beam quality. The optimization method was used to design the proposed S-band high-gradient accelerating structure. In the S-band SW structure, the optimization parameters were the iris shape, iris aperture radius, cavity radius, and coupling hole, and those of the multiple objects were  $ZTT/Q$  (ratio of effective shunt impedance to quality factor),  $E_s/E_a$  (ratio of the actual electric field gradient to the theoretical accelerating gradient),  $H_s/E_a$  (ratio of the actual magnetic field gradient to the theoretical accelerating gradient),  $S_c/E_a^2$  (Poynting vector), and  $\Delta T$  (temperature rise).

SOPF primarily comprises the following steps: In the first step, the performance goals are defined based on the accelerating structure of the design. In the second step, a CST is used to calculate and establish the database, in which several RF properties of the design targets, such as the frequency, temperature rise, input power, and other RF characteristics of the design structure, are correlated with the geometric parameters of the S-band accelerating structure, such as the iris shape, iris aperture radius, cavity radius, and coupling hole size. In the third step, MATLAB

is used to fit an analytic polynomial expression based on the corresponding relationship between different sizes of the accelerated structure and the target physical characteristics of the accelerated structure in the S-band. The goal is to calculate all the physical characteristics of the accelerating structure through the interpolation of the database. In the final step of the SOPF, multiparameter optimization is realized. All parameters of the accelerating structure were determined based on the interpolation operation of the database.

This optimization ensures that the accelerating structure of the S-band converges to the targets under several conditions reflected by the different accelerating structure properties. The convergence is faster, more precise, and automatic compared with that afforded by the traditional optimization.

### 3.1 S-band high-gradient accelerating structure

Based on the RF resonant frequency, the cell lengths and radii of the accelerating structure can be calculated in advance. The cell length  $L$  of the  $\pi$ -mode SW accelerating structure is expressed as

$$L = \beta \frac{c}{2f}, \quad (1)$$

where  $\beta$  is the relativistic velocity of the protons, and  $f$  is the RF frequency of the accelerating structure. In our design, the prototype was 25 cm long, and the geometric  $\beta$  was 0.38. A schematic illustration of the SW accelerating structure is shown in Fig. 2. Figure 2a illustrates the single cavity of the accelerating structure, and the corresponding relationship of each geometric size is shown in Fig. 2a, in which  $x$  and  $y$  are the dimensions of the nose cone,  $h$  the distance from the center of the coupling hole to the center of the beam hole,  $e$  the radius of the coupling hole,  $2a$  the thickness of the accelerating cavity,  $L$  the length of the accelerating cavity, and  $c$  the beam aperture. The S-band accelerating structure comprised 11 cells with a  $\pi$ -mode and a dual-coupler, as shown in Fig. 2b. Figure 2b shows the equivalent parameter values of the first accelerating chamber of the accelerating unit coupler, in which  $b_6$  is the diameter of the coupling cavity, and  $d$  is the narrow side of the WR-284 waveguide. Using the  $\pi$ -mode, a higher shunt impedance and a higher gradient can be obtained [18].

### 3.2 Coupler structure

The accelerating structure comprised accelerating cavities and couplers. The SW accelerating structure designed in this study involved a dual-feed coupler, which transmits RF power to the accelerating cavities by a magnetic coupling hole. The coupler is vital to the operation of the

beam; therefore, the design of the coupler is particularly important.

In designing the coupler, the coupling cavity and accelerating cavity must be matched perfectly. The dual-feed coupler feeds power into the accelerating structure via two ports; therefore, the power at the coupler becomes one-half, and the field at the coupler becomes  $\sqrt{2}/2$ , thereby effectively reducing the maximum field at the coupling hole. As shown in Fig. 2d, the coupling holes between adjacent cavities cross each other, and this can effectively reduce the interference of the next adjacent coupling. The propagation of non-axisymmetric modes should be reduced and the beam load capacity improved. The value of the coupling was 1, and the frequency was 2856 MHz. The design and optimization processes of the dual-feed coupler are introduced next.

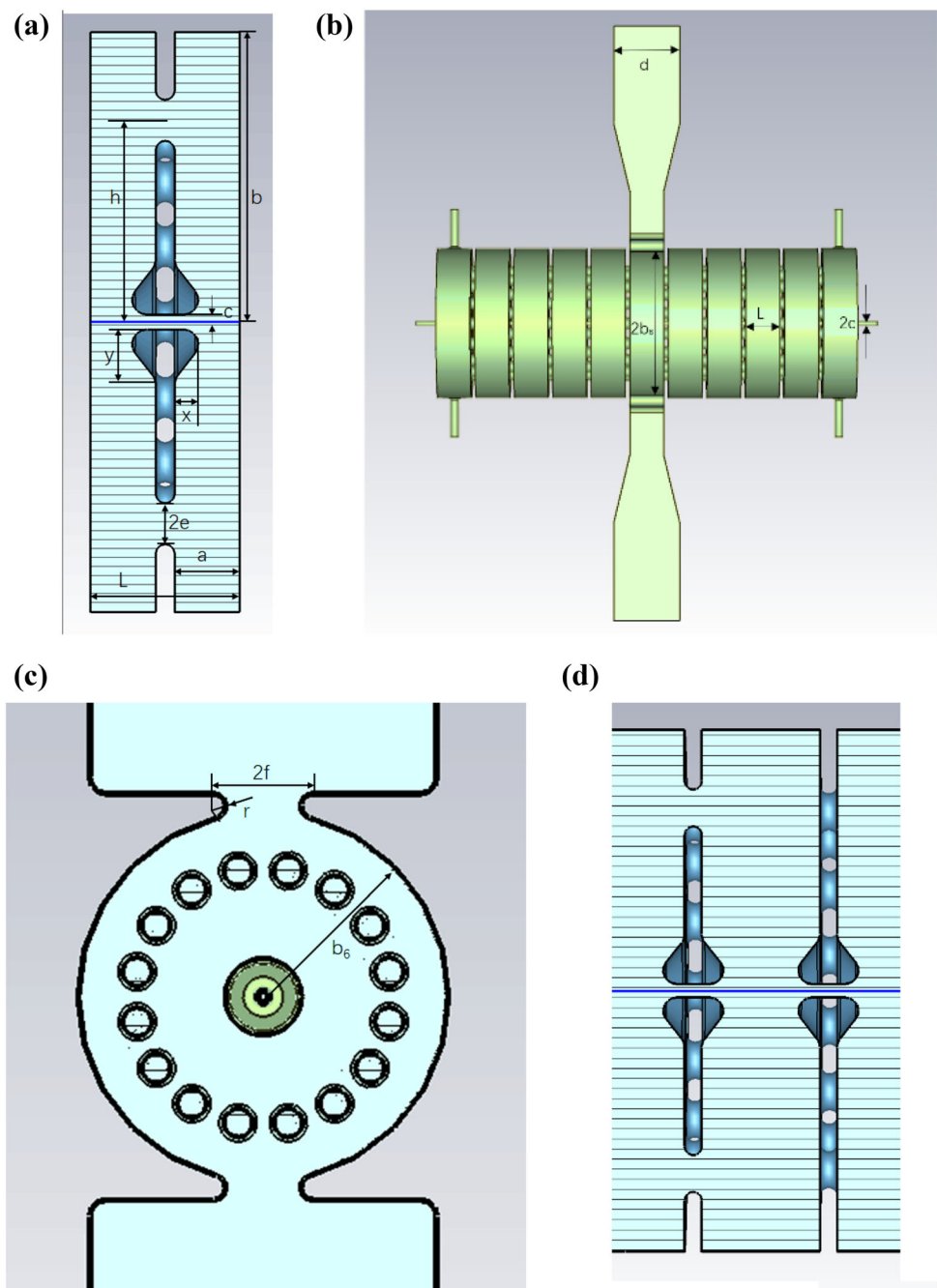
The longitudinal cross section of the dual-feed coupler is shown in Fig. 3, and the transverse cross section is shown in Fig. 2c. The parameters of the coupler cell are presented in Fig. 2c. As shown, the length of the coupling hole is  $2f$ , which is equal to the distance between the two arc centers, where  $r$  is equal to 3 mm, and the coupling cavity radius is  $b_6$ .

### 3.3 Preliminary analysis of acceleration structure

The acceleration model was determined to be a  $\pi$ -mode model at the beginning of the design of this accelerating structure. In this study, when establishing the database of each parameter, as shown in Fig. 2, the sensitivity of each parameter was first analyzed, and an appropriate value was selected for each parameter that was insensitive to frequency. The sensitivity analysis of all the parameters is shown in Table 2. Frequency-sensitive values were obtained by sweeping points. Seven parameters of a single cavity were optimized. Because  $h$  was not sensitive to frequency, we first determined its value. Subsequently, we fixed the values of the parameters above and then changed  $a$  and the nose cone shape separately. Owing to the limitation of the single cavity length calculated based on the RF frequency and value, the value of  $a$  is limited.

After obtaining the sensitivity analysis results from the table above, we established a complete database. The scanning point procedure involved changing the size of the accelerating cavity, and then adjusting the diameter  $b$  of the cavity to ensure a frequency of 2856 MHz, while fixing the other parameters. By analyzing the entire sweep point database, we plotted all the dimensional parameters and physical quantities (as shown in the following figures) as well as normalized all the physical quantities. The normalization involved dividing each physical quantity by its maximum value, and the maximum value of each physical

**Fig. 2** (Color online) Schematic illustration of SW accelerating structure. **a** Single cavity illustration of accelerating structure; **b** schematic diagram of S-band structure comprising 11 accelerating cavities; **c** transverse cross section of dual-feed coupler; **d** coupling holes between adjacent cavities crossing each other



quantity is shown in the figure. As presented in the following figures, the size parameters that exerted a greater effect on each physical quantity were  $a$ ,  $c$ ,  $e$ ,  $x$ , and  $y$ , which correspond to the cavity thickness, beam hole radius, coupling hole radius, and nose cone shape. Hence, we classified the insensitive size parameter  $h$  and selected the appropriate value based on the limit of the physical quantity. The relationship between the sensitive dimensional parameters ( $a$ ,  $c$ ,  $e$ ,  $x$ , and  $y$ ) and physical quantities is shown in Fig. 3a–e, whereas the relationship between the

insensitive dimensional parameter ( $h$ ) and physical quantities is shown in Fig. 3f.

As shown in Fig. 3, the geometric dimensions that significantly affected  $S_e/E_a^2$  and  $E_s/E_a$  were  $a$ ,  $x$ , and  $y$ . The geometric dimension that significantly affected  $\Delta T$  and  $H_s/E_a$  was  $e$ . However, as  $e$  decreased,  $ZTT/Q$  decreased; therefore, we selected  $e = 2.75$  mm as the optimal value. Furthermore, each geometric dimension was insensitive to the physical quantity  $ZTT/Q$ . As shown in Fig. 3d, the beam hole radius ( $c$ ) was insensitive to the physical quantity. Therefore, we selected an appropriate value for  $c$ ,



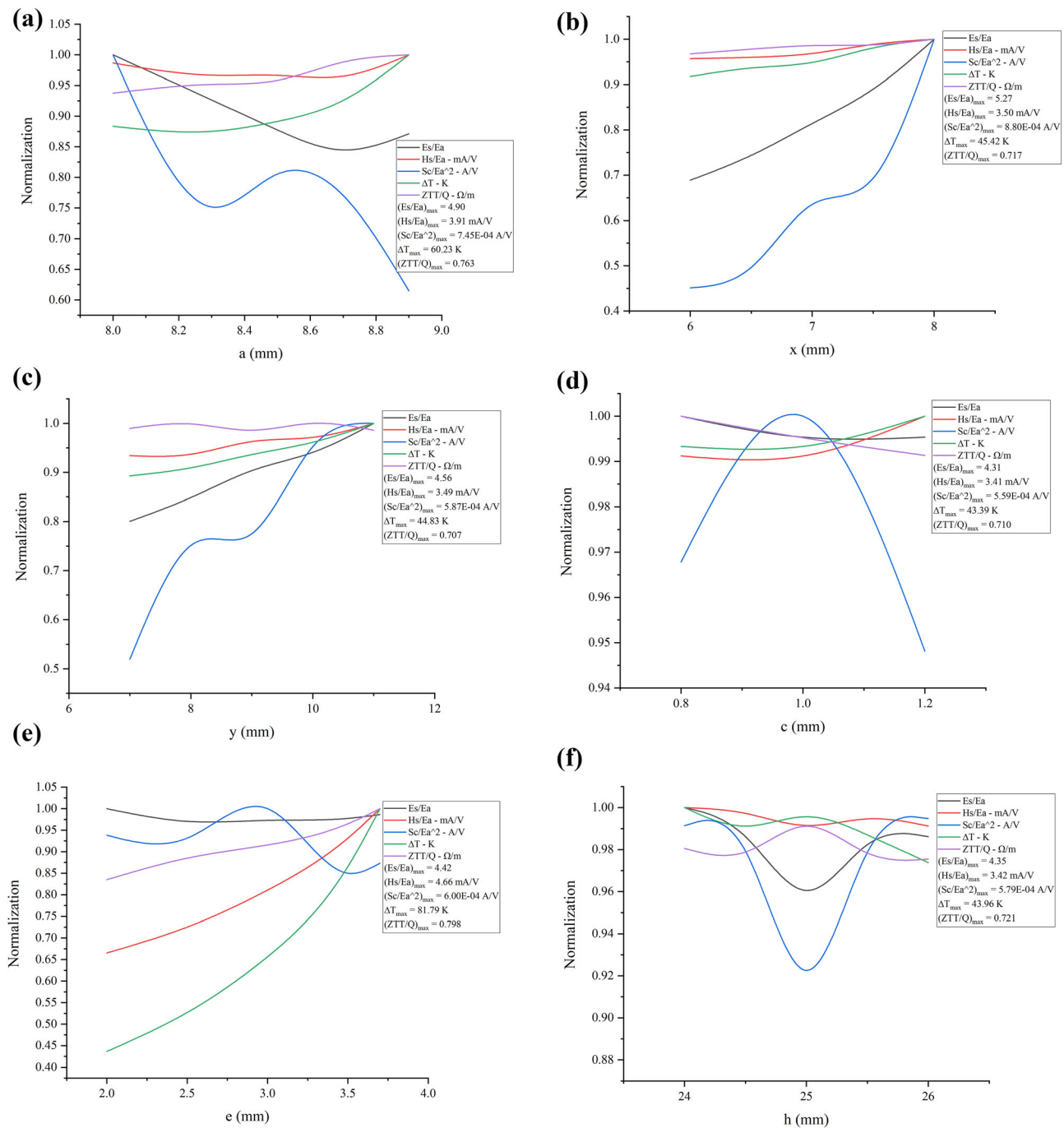


**Fig. 3** (Color online) Relationship between dimensional parameters ( $a$ ,  $x$ ,  $y$ ,  $c$ ,  $e$  and  $h$ ) and physical quantities ( $ZTT/Q$ ,  $E_s/E_a$ ,  $H_s/E_a$ ,  $S_c/E_a^2$ , and  $\Delta T$ ). **a** Variation trend of each physical quantity for various  $a$ ; **b** variation trend of each physical quantity for various  $x$ ; **c** variation

trend of each physical quantity for various  $y$ ; **d** variation trend of each physical quantity for various  $c$ ; **e** variation trend of each physical quantity for various  $e$ ; **f** variation trend of each physical quantity for various  $h$

i.e., 1 mm. As shown in Fig. 3f, the parameter  $h$ , which is the distance between the center of the coupling hole and the center of the beam hole, is not sensitive to any physical quantity. However, the coupling hole size was limited. Combined with the coupling hole size to be provided in the

subsequent analysis, an appropriate value of  $h$ , i.e., 27 mm, was selected.

In summary, we analyzed all the dimensions of the accelerating structure and finally determined the values of the relevant parameters, as follows: beam aperture  $c = 1$  mm; coupling hole radius  $e = 2.75$  mm;  $h = 27$  mm;

**Table 2** Sensitivity analysis of all parameters

Parameter	Step length (mm)	Data range (mm)	Frequency range (MHz)	Sensitivity (MHz/mm)	Number
$a$	0.2	8.0–9.0	2826.40–2877.30	50.897	6
$b$	0.3	35.0–36.5	2920.70–2822.90	65.166	6
$e$	0.2	2.5–3.5	2866.80–2839.60	27.186	6
$h$	0.5	24.0–26.0	2857.10–2855.00	1.063	5
$x$	0.6	5.0–8.0	2988.20–2765.90	74.112	6
$y$	0.5	9.0–11.0	2897.50–2816.60	40.466	5
$c$	0.2	0.8–2.0	2867.20–2802.60	53.849	7

coupling hole chamfer due to processing and manufacturing requirements,  $r_2 = 1.259$  mm (half of the middle thickness plate). Subsequently, the values of  $a$ ,  $x$ , and  $y$  were scanned and optimized. First, a complete database was established based on numerous simulation results. Subsequently, by polynomial fitting, each physical quantity was fitted based on  $a$ ,  $x$ , and  $y$ . The specific optimization process is presented in the following section.

### 3.4 Computational optimization process of S-band high-gradient accelerating structure

Based on the previous analysis, only points of  $a$ ,  $x$ , and  $y$  require scanning and a complete database must be established by polynomial fitting. First, fixed  $x$ ,  $y$ , for there is a linear transformation, step length of 0.2 mm, the range of 8–9 mm, then for each value of  $a$ , is a linear transformation for  $x$ , step length is 0.3 mm, the range of 5–6.2 mm, the following each  $a$  and combination values of  $x$ ,  $y$  have a linear transformation, the step size is 1 mm, the range of 5 to 10 mm. By analyzing the scanning results, we can obtain the fitted polynomial functions of  $ZTT/Q$ ,  $\Delta T$ ,  $E_s/E_a$ ,  $H_s/E_a$ , and  $S_c/E_a^2$ . Subsequently, based on these polynomial functions, parameters  $a$ ,  $x$ , and  $y$  are to be rescanned, and the optimal combination of  $a$ ,  $x$ , and  $y$  that satisfy the requirements of  $ZTT/Q$ ,  $\Delta T$ ,  $E_s/E_a$ ,  $H_s/E_a$ , and  $S_c/E_a^2$  are to be selected. This method can be realized through a simple cycle calculation performed in MATLAB. The procedure is an automatic optimization that yields several groups (distributions of  $a$ ,  $x$ , and  $y$ ) fitting all restrictions among tens of thousands of results by scanning the ranges of  $a$ ,  $x$ , and  $y$ .

### 3.5 Computational optimization process of coupler

In the early stage, the electric field is adjusted by adjusting the cavity diameter without a coupler, which can be achieved easily. When the structure of the coupler was added, the field distribution changed significantly. Owing

to the SW structure, the coupling and reflection conditions differed significantly from those of the traveling wave structure. Therefore, the process of matching and optimizing the accelerating cavity and coupler was complicated.

Because this accelerating structure reflects an SW accelerating proton beam, based on previous experience, it will be extremely difficult to directly calculate the size of the entire accelerating tube. This accelerating structure comprised five target parameters ( $ZTT/Q$ ,  $E_s/E_a$ ,  $H_s/E_a$ ,  $S_c/E_a^2$ , and  $\Delta T$ ) and six structural parameters ( $a$ ,  $x$ ,  $y$ ,  $c$ ,  $e$ , and  $h$ ). Each change in the value of a structural parameter corresponds to a combination of a set of target parameters, which will be an extremely large set of data calculations. In addition, it might not be possible to obtain the optimal combination value of the structural parameters at all times. Therefore, we segmented this process into several steps. The specific process for the optimization is as follows.

First, the intermediate coupling cavity and two semi-cavities on both sides were added. At this stage, the coupling hole, coupling cavity diameter, and diameter of the two semi-cavities can be adjusted easily. In the second step, an entire cavity was added to each side. Based on the first step, the cavity diameter of the newly accelerating cavity was adjusted, and the size of the coupling hole was fine-tuned to achieve the design target. Because the structure was centrally symmetrical, the size of the three acceleration cavities in the middle must be the same. In the third step, three whole cavities were added on each side, and the second step was repeated until the design index was reached. The entire structure was calculated in the final step. Because the edge cavity was added, the effect on the entire structure was prominent. Therefore, many iterative calculations were performed before the design specifications were attained; furthermore, the size of the coupling hole and the diameter of each accelerating cavity were changed. The entire simulation and optimization process was highly dependent on the size. However, the desired result was obtained after performing an involved iterative

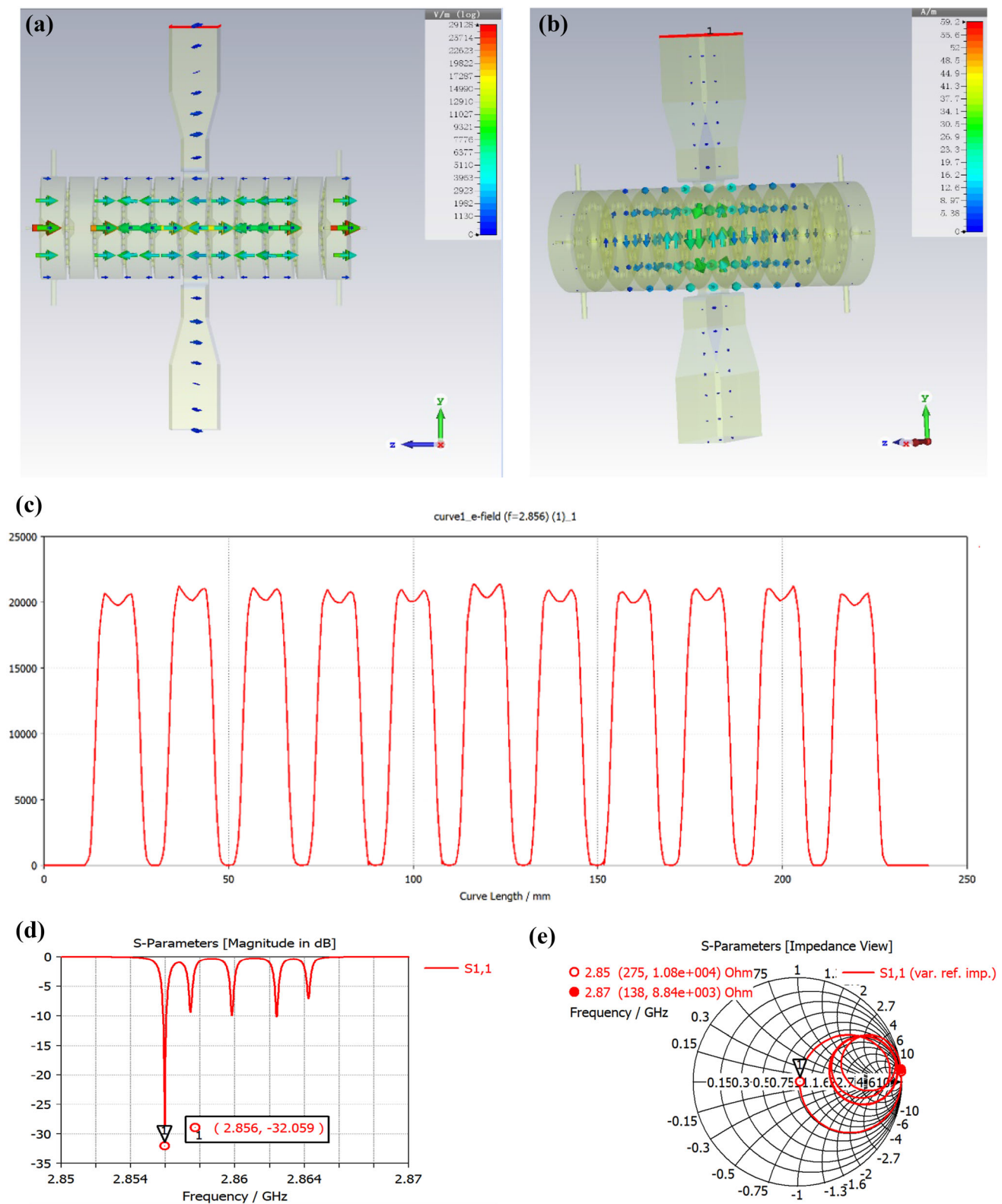


**Fig. 4** (Color online) Final optimization results of entire accelerating structure. **a** Electric field distribution of accelerating structure; **b** magnetic field distribution of accelerating structure; **c** Electric field distribution after adding coupler; **d** S<sub>11</sub> figure; **e** Z Smith chart



process. Figure 4 shows the simulation results for this accelerating structure. Figure 4a, b shows the electromagnetic field distributions of the accelerating structure, where the operating mode is  $\pi$ . The electric field distribution, S11, Z Smith chart are shown in Fig. 4c–d, respectively. The value of S11 was  $-32.059$  dB at 2856 MHz, and the coefficient of coupling was 1. The deviation in the balance of the electric field was less than 1%.

### 3.6 Final optimization result

Using an efficient method (polynomial fitting) to complete the automatic optimization at the beginning of the establishment and analysis of the database, it was concluded that a series of parameters, as shown in Table 3, satisfied the design requirements for the S-band high-gradient proton accelerating structure.

## 4 Fabrication, low-power RF tests, and preparation

In this section, the manufacturing details and brazing processes of the accelerating structure are briefly described, and low-power RF measurements and tuning are discussed. Figure 5 shows the SW high-gradient accelerating structure before and after processing. A three-dimensional model sketch of the first S-band accelerating structure for a proton therapy linac is shown in Fig. 5a, and the processed accelerating structures are shown in Fig. 5b, c. Next, we

introduce the process of manufacturing and brazing as well as the cold test experiment in two separate subsections.

## 5 Fabrication and brazing of accelerating structure

This proton-accelerating structure is the first prototype created at our proton therapy facility; therefore, previous manufacturing experience for its support and accumulation is lacking. We eventually decided to use a two-step approach. The first step is to manufacture the sample chamber, where a few representative bowl cavities are selected to investigate the fabrication, measurement, and brazing processes. All the accelerating cells were made of oxygen-free copper. A single accelerating cavity is shown in Fig. 5b, and the assembled accelerating unit is shown in Fig. 5c. It is composed of two H-Bends, a power divider, and an accelerating structure. It was installed on a Shanghai soft X-ray free-electron laser device for high-power experiments. By analyzing and summarizing the deficiencies of the brazing process and the processing of proton accelerating structures, we discovered an improvement technique that will benefit the formal processing of proton accelerators. The second step is to manufacture a formal accelerating structure.

### 5.1 Cold testing experiment of accelerating structure and result analysis

We used a network analyzer and a stepper motor to pull the cable, and a bead-pull measurement method to perform the microwave measurement experiments. A network analyzer was used to measure the coupling coefficient and SW ratio of the accelerating structure, as well as the S-parameter. The bead-pull method was used to measure the electric field distribution using an existing mature measurement platform, and the measurement principle is available in Ref. [19]. Finally, we flattened the field distribution through multiple adjustments (pulling and pushing) of the tuning screw to change the diameter of the accelerating cavity. The measurement result for the size was highly sensitive to the tuning; therefore, the tuning process was extremely complicated. Through many adjustments, the final cold test result of the accelerating structure of this high-gradient compact linac device for advanced proton therapy was obtained, as shown in Fig. 6. The final field distribution of the accelerating structure is shown in Fig. 6a. The amplitude of the fourth peak was low because the tuning hole of the fourth cavity was damaged by the mechanical force during tuning, which prevented further tuning. The deviation in the balance of the electric field was approximately 3%, which was

**Table 3** Parameters of SW accelerating structure obtained from automatic optimization

Frequency, $f$ (MHz)	2856
Operating mode	$\pi$
Cell No	11
Effective length (mm)	219.538
Cell length, $L$ (mm)	19.958
Iris thickness, $(L-2a)$ (mm)	2.518
Diameter, $2b$ (mm)	77.706
Beam aperture radius, $c$ (mm)	1
Cavity thickness, $a$ (mm)	8.72
Coupling hole radius, $e$ (mm)	2.75
Quality factor, $Q$	9138
Relative maximum magnetic field, $H_z/E_a$ (mA/V)	3.457
Shunt resistance, $Z_{IT}$ (M $\Omega$ /m)	59.983
Temperature rise (K)	43.73
Filling time, $t_f$ ( $\mu$ s)	0.257
Revised poynting vector, $S_z/E_a^2$ (A/V)	$2.635 \times 10^{-4}$
Relative maximum electric field, $E_z/E_a$	2.899

**Fig. 5** (Color online) SW accelerating structure. **a** Three-dimensional model sketch of S-band high-gradient accelerating structure; **b** S-band high-gradient accelerating cavity; **c** assembled accelerating unit

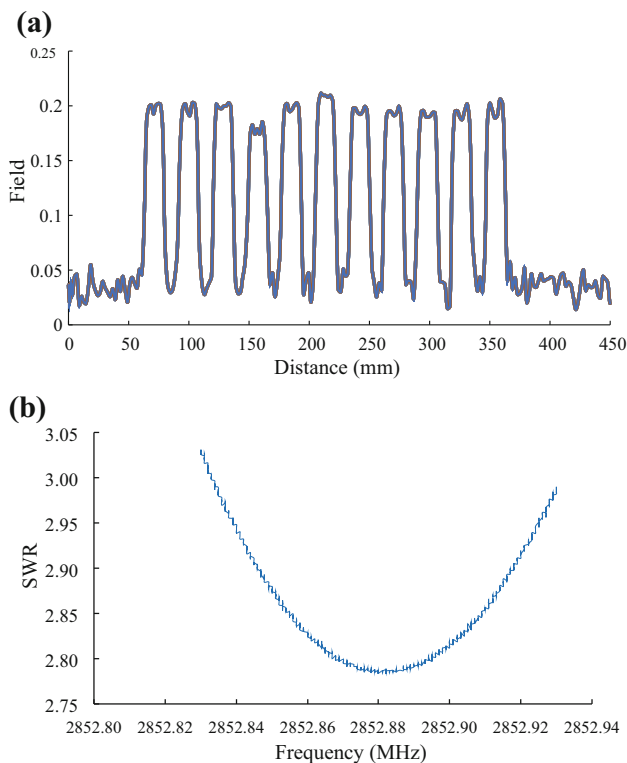
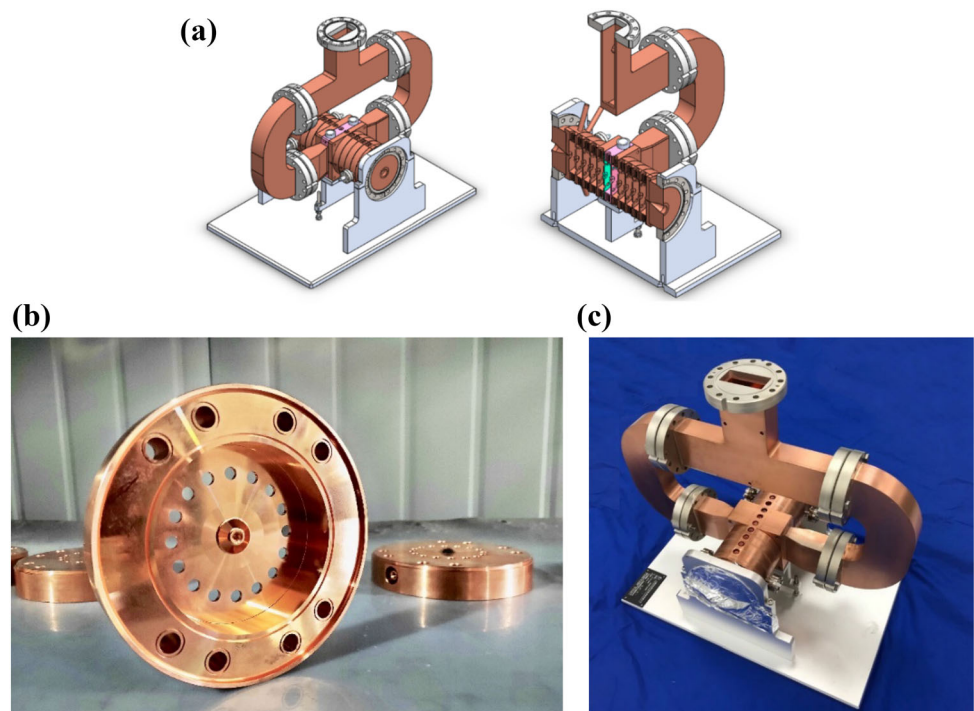


**Fig. 6** Final cold test results (field distribution, SWR, and frequency). **a** Field distribution of accelerating structure; **b** SWR measurement result of entire accelerator tube, SWR = 2.78

significantly affected by the coupling coefficient. The measurement results of the final SW ratio (SWR) and

coupling coefficient of the entire accelerator tube are shown in Fig. 6b. The SWR was 2.78, which resulted in a significant power reflection. In the first prototype, the field distribution was extremely sensitive to cavity size changes during tuning. Owing to machining errors, the mismatch between the coupling and accelerating cavities resulted in an increase in reflection. To ensure that the field distribution was flat, we determined the SWR and discovered that it was higher than the typical SWR. For high-power tests to be performed in the future, we can protect the power source using a circulator to absorb the reflected power, or use the klystron to feed more power to attain the operating power. The final measurement operating frequency of this accelerating structure was 2852.88 MHz, and the S-parameter in the frequency range was  $-6.57$ . The frequency deviation of the accelerating structure can be rectified by adjusting the temperature of the cooling water. Finally, a series of surface treatments were performed, including manual polishing and painting. Finally, it was packed and transported to the laboratory to be subjected to subsequent high-power experiments, which will not be explained in detail in this section.

## 6 Conclusion

In this study, the prototype of an S-band accelerating structure dedicated to advanced proton therapy was developed for a proton therapy linac. Its design, fabrication, and brazing were explained, as well as the cold tests

performed on it. It is noteworthy that the tuning process resulted in a complicated SW accelerating structure. The results of the low-power test showed that the prototype after fabrication and tuning was consistent with our design; therefore, it can significantly promote the development of an advanced facility for proton therapy. In the later stage, a high-power test and a beam test will be conducted to verify the appropriate accelerating gradient for a proton linac. In conclusion, the prototype was successfully fabricated. In particular, the  $\pi$ -mode determined using only the same cell array was sensitive to fabrication and tuning. Therefore, it will be optimized and evolved into a better design based on an alternative cell array for a more stable production and operation. Furthermore, we will strive for compactness and high dose rates in the future.

**Author contributions** All authors contributed to the study conception and design. Material preparation, data collection and analysis were performed by Yu Zhang, Wen-Cheng Fang, Xiao-Xia Huang, Jian-Hao Tan, Cheng Wang, Chao-Peng Wang and Zhen-Tang Zhao. The first draft of the manuscript was written by Yu Zhang and all authors commented on previous versions of the manuscript. All authors read and approved the final manuscript.

## References

1. R.R. Wilson, Radiological use of fast protons. *Radiology* **47**, 487–491 (1946). <https://doi.org/10.1148/47.5.487>
2. R.C. Han, Y.J. Li, Y.H. Pu, Collection efficiency of a monitor parallel plate ionization chamber for pencil beam scanning proton therapy. *Nucl. Sci. Tech.* **31**, 13 (2020). <https://doi.org/10.1007/s41365-020-0722-z>
3. Particle Therapy Cooperative Group (PTCOG) Collaboration. <http://www.ptcog.com>
4. R.S. Zheng, K.X. Sun, S.W. Zhang et al., Analysis on the prevalence of malignant tumors in China in 2015. *Chin. J. Oncol.* **41**, 19–28 (2019). (in Chinese)
5. P. Montay-Gruel, A. Bouchet, M. Jaccard et al., X-rays can trigger the FLASH effect: ultra-high dose-rate synchrotron light source prevents normal brain injury after whole brain irradiation in mice. *Radiother. Oncol.* **129**, 582–588 (2018). <https://doi.org/10.1016/j.radonc.2018.08.016>
6. R.W. Hamm, K.R. Crandall, J.M. Potter, Preliminary design of a dedicated proton therapy linac, in *Conference Record of the 1991 IEEE Particle Accelerator Conference*, (San Francisco, CA, USA, 1991), pp. 2583–2585. <https://doi.org/10.1109/PAC.1991.165037>
7. A.J. Lennox, Hospital-based proton linear accelerator for particle therapy and radioisotope production. *Nucl. Instr. Methods Phys. Res. A* **56–57**, 1197–1200 (1991). [https://doi.org/10.1016/0168-583X\(91\)95130-6](https://doi.org/10.1016/0168-583X(91)95130-6)
8. U. Amaldi, P. Berra, K. Crandall et al., LIBO—alinac—booster for proton therapy: construction and test of a prototype. *Nucl. Instr. Methods Phys. Res. A* **521**, 512–529 (2004). <https://doi.org/10.1016/j.nima.2003.07.062>
9. C. Ronsivalle, A. Ampollini, G. Bazzano et al., The Top Implant Linac: machine status and experimental activity, in *Proceedings of IPAC2017. ENEA C.R. Frascati, Frascati (Roma), Italy*. <https://doi.org/10.18429/JACoW-IPAC2017-THPVA090>
10. S. Benedetti, A. Grudiev, A. Latina, High gradient linac for proton therapy. *Phys. Rev. Accel. Beams* **20**, 040101 (2017). <https://doi.org/10.1103/PhysRevAccelBeams.20.040101>
11. H.Y. Li, X.M. Wan, W. Chen et al., Optimization of the S-band side-coupled cavities for proton acceleration. *Nucl. Sci. Tech.* **31**, 23 (2020). <https://doi.org/10.1007/s41365-020-0735-7>
12. X.X. Huang, W.C. Fang, Q. Gu et al., Design of an X-band accelerating structure using a newly developed structural optimization procedure. *Nucl. Instrum. Methods Phys. Res. A* **834**, 45–52 (2017). <https://doi.org/10.1016/j.nima.2017.02.050>
13. A. Degiovanni, R. Bonomi, M. Garlasché et al., High gradient rf test results of S-band and C-band cavities for medical linear accelerators. *Nucl. Instrum. Methods Phys. Res. A* **890**, 1–7 (2018). <https://doi.org/10.1016/j.nima.2018.01.079>
14. A. Degiovanni, High gradient proton linacs for medical applications, Ph.d. thesis, EPFL (2014). <https://doi.org/10.5075/epfl-thesis-6069>
15. A. Degiovanni, U. Amaldi, R. Bonomi et al., TERA high gradient test program of rf cavities for medical linear accelerators. *Nucl. Instrum. Methods Phys. Res. A* **657**, 55–58 (2011). <https://doi.org/10.1016/j.nima.2011.05.014>
16. S. Benedetti, A. Ugo, D. Alberto et al., RF design of a novel S-band backward traveling wave linac for proton therapy, in *Proceeding of 27th Linear Accelerator Conference, Geneva, Switzerland*. THPP061 (2014). <http://cds.cern.ch/record/2062620>
17. S. Benedetti, T. Argyropoulos, C.B. Gutiérrez et al., Fabrication and testing of a novel S-band backward traveling wave accelerating structure for proton therapy linacs, in *Proceedings of the 28th Linear Accelerator Conference, East Lansing, MI, USA*, (2016). <https://doi.org/10.18429/JACoW-LINAC2016-MOPLR048>
18. Y. Nour, T. Abulfadl, Design of X-band medical linear accelerator with multiple RF feeds and RF phase focusing, in *Proceedings of IPAC2013, Shanghai, China* (2013). <https://accelconf.web.cern.ch/IPAC2013/papers/thpwa001.pdf>
19. P.-F.R. Gapais, Bead-Pull measurements techniques and Multipoles components of DQW crab-cavity. *CERN Summer Student 2018 Report*. CERN-STUDENTS-Note-2018–144 <https://cds.cern.ch/record/2638938>